Dalton Transactions

COMMUNICATION

View Article Online
View Journal | View Issue

Cite this: *Dalton Trans.*, 2019, **48**, 1941

Received 18th September 2018,
Accepted 20th December 2018

DOI: 10.1039/c8dt03776k

rsc.li/dalton

Energy storage inspired by nature – ionic liquid iron–sulfur clusters as electrolytes for redox flow batteries †

Christian Modrzynski and Peter Burger *

The redox flow battery (RFB) is a promising technology for the storage of electric energy. Many commercial RFBs are often based on acidic vanadium electrolyte solutions that have limitations regarding stability and energy density. Here, a new approach is presented that is inspired by nature's electron storage, *i.e.* iron–sulfur clusters $[Fe_4S_4(SR)_4]^{2-}$. In combination with imidazolium cations, new ionic liquid electrolyte materials were obtained and characterized with regard to their physico- and electrochemical properties. For flow battery tests, the bromide/bromine redox-couple was used in the second half cell in an ionic liquid solution. In these measurements, liquid iron–sulfur clusters show high coulombic (>95%) and energy (69%) efficiencies combined with a high theoretical energy density (88 W h L^{-1}).

Introduction

The increasing share of renewable energies leads to an intermittent generation of electric energy. Therefore, it is necessary to provide ways for efficient energy storage, which requires high energy and power densities. Furthermore, a high cycling stability and a low price are targets. Here, the redox flow battery (RFB) is a promising technology. The separated electrolyte tanks ensure a low self-discharge and independent scaling of power and energy outputs up to multi-MW/MWh systems.[1] Today's most commonly applied all-vanadium RFBs, however, suffer from a low energy density of max. 40 W h L^{-1} (ref. 2) compared to Li ion batteries that reach up to ~700 W h L^{-1}.[3,4] Recently, new RFB systems have been described using metal complexes or organic substances in aqueous or non-aqueous solution.[5–18] The focus of many studies is on energy density but costs, stability, membrane selectivity and current density are also investigated. The maximum theoretical energy density is proportional to the number of transferred electrons n, the concentrations of the electrolytes c and the potential difference of the two half cells ΔE. This provides three possibilities to improve the energy density:

(i) To increase ΔE, the electrochemical window of the solvent must be wide; therefore water is a limiting factor. Here, ionic liquids (ILs) show great potential due to their wide electrochemical window.[19,20]

(ii) High concentrations can be achieved if the redox active component is part of the IL as one of its ions. Only two such systems have been described in the literature so far, *i.e.* a semi-flow battery that deposits copper[21] and two systems using liquid metal salts[22] or organic anions.[23] However, the energy density is not discussed in the latter publication. Therefore, we targeted new redox active ionic liquids with high potentials.

(iii) Finally, the number of transferred electrons per molecule can be increased. This was utilized by the application of different polyoxometalates (POMs)[24–29] and organic molecules[5,15,30–32] but often due to low concentrations, only low energy densities were achieved.

With respect to these considerations, liquid iron–sulfur cluster salts are proposed as a high energy density electrolyte. These clusters $[Fe_4S_4(SR)_4]^{n-}$ (Fig. 1) are well-known from ferredoxin-proteins and serve as electron reservoirs in nature for

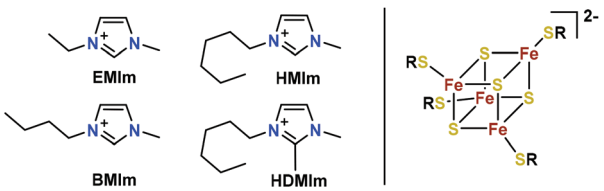

Fig. 1 Ionic liquid cations (left) and the general structure of cubane-type iron–sulfur clusters (right).

Institut für Anorganische und Angewandte Chemie, Department Chemie, Universität Hamburg, Martin-Luther-King-Platz 6, 20146 Hamburg, Germany. E-mail: burger@chemie.uni-hamburg.de

†Electronic supplementary information (ESI) available: Experimental details, syntheses, scan-rate-dependent CVs of $[Fe_4S_4(Stfe)_4]^{2-}$, Randles–Ševčík-plots, TGA-plots, conductivity- and viscosity-data, NMR-spectra and X-ray-data. CCDC 1573434 and 1573435. For ESI and crystallographic data in CIF or other electronic format see DOI: 10.1039/c8dt03776k

numerous purposes.[33] They are composed of four iron atoms that are bridged by four μ^3-sulfido-ligands and coordinated by a variable thiolato ligand (RS^-). They are known to exist in four different oxidation states, making them interesting for energy storage (*cf.* iii)). Additionally, the high abundance of iron and sulfur makes them attractive, inexpensive and environment friendly energy storage materials. By the combination of the anionic clusters with IL cations (Fig. 1), liquids with promising electrochemical properties are anticipated.

The use of ILs is emphasized by their beneficial properties like low volatility, non-flammability, good thermal and chemical stability and intrinsic conductivity.[34–40] The large amount of different ILs offers numerous possibilities for the synthesis of ILs with specific properties. Therefore, ILs are highly interesting for RFB applications;[41] however only a few IL-based systems have been reported so far.[23,42,43] Additionally, in comparison with acidic and aqueous electrolytes, like the classic vanadium system, ionic liquids are not corrosive and thus allow the use of less robust materials (*e.g.* pump, tank, and tubing). Also they are inflammable and non-volatile in contrast to the recently applied organic solvents resulting in a saver application.

Already known ILs with multi-electron transfers are POM-based.[44,45] Such ILs were also previously investigated by our group;[46] however, due to their low intrinsic energy density, they were not further considered for RFB applications. Other multimetallic systems besides POMs are rare, but a few with oligomeric structures[30,31] were reported that aim for an increase in the number of electrons or larger structures to prevent crossover.

Results and discussion

Synthesis

The preparation of iron–sulfur clusters is well established.[47] A sodium thiolate is reacted with $FeCl_3$ and sulfur forming $[Fe_4S_4(SR)_4]^{2-}$ in solution, which can be isolated by the addition of an appropriate organic cation. To obtain ionic liquids, we chose suitable cations, *e.g.* imidazolium salts. In a synthetically more simple procedure, the tetramethylammonium (TMA) salt of the cluster with R = Me was prepared at first and characterized by NMR and X-ray crystal structure analysis (*cf.* the ESI†). The cation can be exchanged afterwards by a typical IL cation (eqn (1)). With imidazolium cations, cluster salts were obtained as room temperature ILs and characterized (Scheme 1). However, apparent high viscosities make them unsuitable for RFBs.

It is known that ILs with low viscosity often contain fluorinated anions, *e.g.* BF_4^- and PF_6^-.[48] Therefore, a new cluster with a fluorinated thiolato ligand was sought. In this case, 2,2,2-trifluoroethanethiol was used to prepare the cluster $[Fe_4S_4(Stfe)_4]^{2-}$ (Stfe = trifluoroethanethiolate) by refluxing a solution of $[Fe_4S_4(SMe)_4]^{2-}$, while removing gaseous methanethiol from the reaction mixture (eqn (2)). The X-ray crystal structure[49] of the TMA salt of $[Fe_4S_4(Stfe)_4]^{2-}$ (Fig. 2) shows the typical structural characteristics of cubane iron–sulfur clusters.[50]

$$(Me_4N)_2[Fe_4S_4(SR)_4] + EMImBr \xrightarrow[\text{MeCN}\ -Me_4NBr]{\text{15 min.}} (EMIm)_2[Fe_4S_4(SR)_4] \quad (1)\ 84\ \%$$

$$(Me_4N)_2[Fe_4S_4(SMe)_4] + CF_3CH_2SH \xrightarrow[\text{THF}\ -MeSH]{\text{18 h, reflux}} (Me_4N)_2[Fe_4S_4(Stfe)_4] \quad (2)\ 89\ \%$$

Scheme 1 Synthesis of iron–sulfur cluster based ionic liquids.

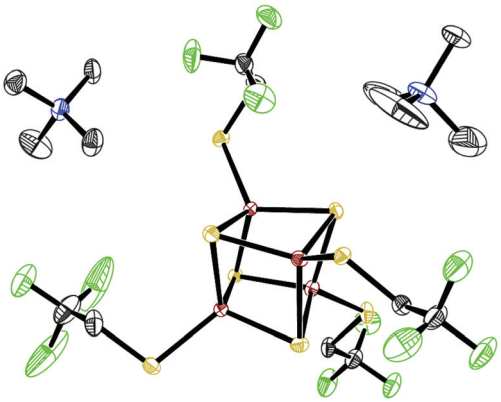

Fig. 2 ORTEP-plot (50%) of $(Me_4N)_2[Fe_4S_4(SCH_2CF_3)_4]$. A co-crystallized THF molecule and the hydrogen atoms are omitted for clarity (● Fe, ● S, ● F, ● N, ● C).

Thermo- and physicochemical properties

After cation exchange, several liquids could be obtained. Their melting points were determined by differential scanning calorimetry (Table 1). These salts undergo glass transitions at temperatures between −30 °C and −50 °C. The Stfe-cluster salts show glass transition temperatures T_g lower than those of SMe-cluster salts. As it is known for imidazolium ILs, T_g increases with increasing alkyl chain-length and decreases with methyl substitution in the 2-position.[34] The first trend is not observed in this case; however, such a behavior has been reported for other imidazolium ILs.[51]

The thermal stability of the EMIm- and TMA-salts of $[Fe_4S_4(Stfe)_4]^{2-}$ was investigated by thermogravimetric analysis (TGA), which proved that the salts are stable up to 150 °C. For the application of an ionic liquid in an RFB, its viscosity is also an important parameter. At room temperature, $(EMIm)_2$-$[Fe_4S_4(Stfe)_4]$

Table 1 Glass transition temperatures of IL iron–sulfur clusters [°C]

	Cation			
Thiolate	EMIm	BMIm	HMIm	HDMIm
SMe	−42	−39	−41	−32
Stfe	−45	−50	−50	−49

has a viscosity of 1800 mPa s, which decreases significantly to 366 mPa s at 50 °C and further to 117 mPa s at 80 °C. The electric conductivity of neat $(EMIm)_2[Fe_4S_4(Stfe)_4]$ was determined at different temperatures reaching from 0.16 mS cm^{-1} at 18 °C to 5.81 mS cm^{-1} at 101 °C. These values are typical of ionic liquids,[39,52,53] but are below those of aqueous systems.[54] This can lead to a higher cell resistance in the RFB.

The electrochemistry of $[Fe_4S_4(Stfe)_4]^{2-}$ was investigated by cyclic voltammetry (Fig. 3). In THF, two quasi-reversible reductions (ΔE_{p1} = 97 mV, ΔE_{p2} = 190 mV at 100 mV s^{-1}) can be observed at −1.55 V and −2.23 V *vs.* Fc/Fc^+. The measurement of multiple cycles did not alter the shape of the CV-curve, confirming reversibility (s. ESI, Fig. S4†). In ILs, the redox-potentials obtained from the CV are shifted towards more positive potentials (s. ESI, Fig. S3†).

The rate constants of the reduction processes were determined according to the Nicholson method[55] from the peak separation in the CV. In $EMImNTf_2$, the first reduction has a rate constant of 5.1×10^{-3} cm s^{-1}, while the second reduction shows a rate constant of 4.1×10^{-3} cm s^{-1}. In acetonitrile, the rate constants are 0.91×10^{-2} cm s^{-1} and 0.78×10^{-3} cm s^{-1} for the first and second reduction, respectively. This fast electron transfer is common in non-aqueous media in contrast to many aqueous systems, *e.g.* vanadium electrolytes, where slower kinetics are frequently observed.[8,12,56]

This reversibility in ILs and the strongly negative redox potentials support the application of iron–sulfur clusters as a redox-active ionic liquid RFB electrolyte.

Flow battery measurements

To investigate the iron sulfur cluster in an RFB, the bromide/bromine redox couple was used as the positive electrolyte in ionic liquid solution (Scheme 2). The Br^-/Br_2 couple – or in excess of Br^-, the Br^-/Br_3^- couple – is well-known from the aqueous Zn/Br-RFB; however, it was not applied in an IL-medium previously. This results in a cell voltage of 1.4 V. For initial tests, a 0.1 M solution of $(EMIm)_2[Fe_4S_4(Stfe)_4]$ and a 0.15 M solution of EMImBr in $EMImNTf_2$ were used in the respective half-cells. Both half-cells were separated using an F-14100 (FuMATech) cation exchange membrane. This cell was charged with 1 mA cm^{-2} until the first reduction step of the

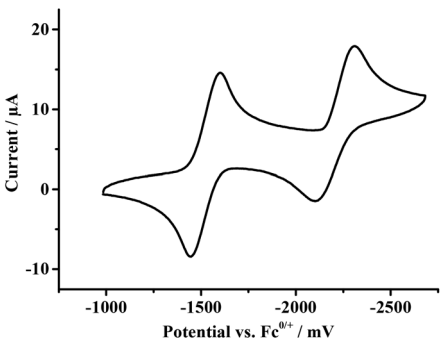

Fig. 3 Cyclic voltammogram of $[Fe_4S_4(Stfe)_4]^{2-}$ (*vs.* Fc/Fc^+), THF (0.1 M nBu_4NPF_6), 100 mV s^{-1}.

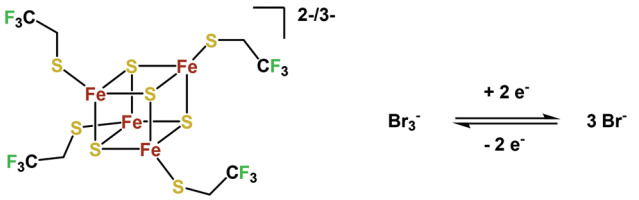

Scheme 2 Redox-reactions of the iron–sulfur cluster ionic liquid RFB.

cluster was completed using cut-offs at 1.8 V and 0.5 V as limits. This results in a relatively high energy efficiency (EE) of 69% (Fig. 4b), which is comparable with that of other RFB systems.[5–12,21,57] It must be emphasized that the applied membrane is optimized for proton transport and not for the much larger imidazolium cations, which impedes the application of higher current densities in combination with the moderate conductivity of ILs. The coulombic efficiency (CE) is at a high level at about 95% considering the early stage of development. With the Br^-/Br_3^- half-cell, a maximum theoretical energy density of approximately 70 W h L^{-1} (for calculations see ESI, eqn (4)†) can be reached considering that the neat ionic liquid $(EMIm)_2[Fe_4S_4(Stfe)_4]$ has a 1.5 M concentration and a 3 M concentration of EMImBr in $EMImNTf_2$ is possible. With the room temperature IL HMImBr which is 5 M, the energy density can be increased to 88 W h L^{-1}. This value could certainly be even further improved by using a catholyte with a more positive potential.

The charge/discharge behavior was investigated at different current densities in order to improve the performance of the battery. By increasing the current density up to 5 mA cm^{-2}, the charge and discharge potentials are shifted towards higher and lower potentials, respectively (Fig. 4c).

Due to this, the energy efficiency is decreased to 56% at 2 mA cm^{-2} and further to 33% at 5 mA cm^{-2} (Fig. 4d). The coulombic efficiency is not affected by current density though.

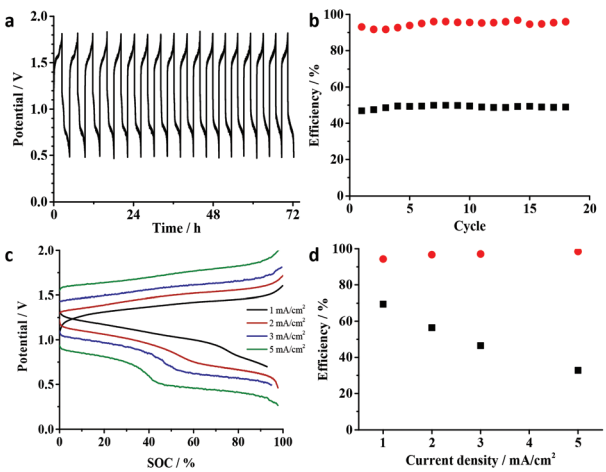

Fig. 4 (a) Charge/discharge voltage-profile at 1 mA cm^{-2} with 0.1 M $(EMIm)_2[Fe_4S_4(Stfe)_4]$ and (b) the corresponding coulombic (●) and energy (■) efficiencies. (c) Charge/discharge voltage-profiles at different current densities (SOC: state of charge) and (d) the corresponding coulombic (●) and energy (■) efficiencies.

In order to demonstrate that ionic liquid electrolytes can be applied for RFBs with high energy density, $(EMIm)_2[Fe_4S_4(Stfe)_4]$ was used in 1.0 M concentration. Note that this is close to the concentration of the neat redox-active IL of 1.5 M. The measurements were performed at 50 °C to decrease the viscosity of the ionic liquid and at the same time increase its conductivity. The obtained charge/discharge profile (Fig. 5) shows a similar behavior to that of the diluted sample. However, the CE is decreased to approximately 80% in the first cycles, but increases afterwards and reaches 95% after 15 cycles. As a result of the lower CE, a decrease in EE to 60% is observed. In contrast to the increase in CE during the measurement, the EE decreases over time. This effect is most likely caused by the degradation of the membrane causing a higher cell resistance and therefore energy losses. This increased cell resistance could be observed by impedance spectroscopy (see ESI, Fig. S7†).

The behavior of the 0.1 M electrolyte was investigated by ^{19}F NMR spectroscopy. The paramagnetic shift of the ^{19}F NMR signal of the trifluoroethyl group provides insight into the species present during cycling. While charging the battery, new signals at −2.4 ppm and −55.3 ppm were observed and assigned to $[Fe(Stfe)_4]^{2-}$ and $[Fe_3S_4(Stfe)_2]^{2-}$ corresponding to the dismutation of the reduced cluster. This is in contrast to the expected formation of $[Fe_4S_4(Stfe)_4]^{3-}$, nevertheless upon discharging, $[Fe_4S_4(Stfe)_4]^{2-}$ was restored. During the second cycle, the aforementioned complexes were again formed and in addition $[Fe_6S_9(Stfe)_2]^{2-}$ was generated, as well as non-coordinated $tfeS^-$. These processes explain the non-ideal shape of the charge/discharge profile. This behavior is in contrast to the CV data as well as the bulk electrolysis experiments in acetonitrile, which led to the isolation of $(Bu_4N)_3[Fe_4S_4(Stfe)_4]$ (s. ESI†). This species was characterized and found to be stable for weeks. So far this differing behavior in the flow cell remains unaccounted, but is further investigated. This flexibility of iron–sulfur cluster structures prevents actual decomposition especially since $[Fe_4S_4(Stfe)_4]^{2-}$ is known to be a thermodynamic sink in iron–sulfur–thiolate chemistry[50,58,59] and thus can be reformed.

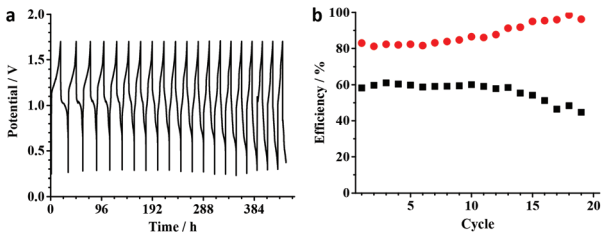

Fig. 5 (a) Charge/discharge voltage-profile at 1 mA cm^{-2} with 1.0 M $(EMIm)_2[Fe_4S_4(Stfe)_4]$ and (b) the corresponding coulombic (●) and energy (■) efficiencies.

Another issue that may lead to a capacity decrease is the crossover of bromide or tribromide ions through the membrane. For hydrogen–bromine cells, crossover rates in the range of 10 mg h^{-1} cm^{-2} were reported[60,61] that were confirmed for quinone–bromine RFBs.[62] These values may be in the same range for ILs as well and therefore could contribute to the capacity decay. Thus, this issue will receive further attention in our research concerning the improvement of cell performance.

A comparison with other multimetallic electrolytes is given in Table 2. This shows that the presented ionic liquid electrolyte possesses a higher theoretical energy density than most

Table 2 Multimetallic RFB electrolyte systems and their energy density, current density and energy efficiency

System	Theor. ED[a] [W h L^{-1}]	Appl. ED[b] [W h L^{-1}]	J [mA cm^{-2}]	EE [%]	Ref.
$[SiV_3W_9O_{40}]^{10-}$ $[SiV_3W_9O_{40}]^{10-}$	≈73	1.6	2.0	≈30	24
$[Co_6S_8(PTA)_6]$ Methylviologene	1.5	0.023	≈0.1	≈50	63
$[CoW_{12}O_{40}]^{6-}$ $[CoW_{12}O_{40}]^{6-}$	15.4	15.4	25–100	86	25
$[SiW_{12}O_{40}]^{4-}$ $[PV_{14}O_{42}]^{9-}$	?	≈7	30–60	70	26
$[TiV_5O_6(OMe)_{13}]^-$ $[TiV_5O_6(OMe)_{13}]^-$	15.8	0.16	0.015	≈50	27
$[P_2W_{18}O_{62}]^{6-}$ Br^-	1000	225	50	76	28
$[V_6O_7(OR)_9(OCH_2)_3R']$ $[V_6O_7(OR)_9(OCH_2)_3R']$	14.6	8.6	0.4	45	29
Perylene diimide $C(O(CH_2)_6Fc)_4$	20.0	4.6	1.16	68	30
$EMIm_2[Fe_4S_4Stfe)_4]^{2-}$ Br^-	87.7	43.6	1.0	69	Herein

[a] Maximum possible energy density calculated with the maximum solubility and redox-potentials. [b] Applied energy density in a test cell calculated with the utilized concentrations.

systems as well as one of the highest demonstrated energy densities. The achieved current density is relatively low; however, this is not uncommon for non-aqueous systems in the early stage of development. The energy efficiency is also sufficiently high and in the same range of other systems. Only the remarkable system of Cronin *et al.*[28] which was only recently published shows a significantly higher energy density than every other RFBs.

In comparison with aqueous all-vanadium RFBs, a significant increase in energy density is achieved. However, the accessible current density is two orders of magnitude lower than that for vanadium systems.

Conclusions

In summary, for the first time, nature's electron storage iron–sulfur clusters were adopted for energy storage in RFBs. For this purpose, new room temperature ionic liquids were prepared and characterized. Their electro- and physicochemical properties were investigated, showing two redox waves, a sufficient viscosity and conductivity. Together with their high thermal stability, these redox-active ionic liquids are promising electrolytes for one of the first IL-based RFBs. In combination with a bromide/tribromide based IL, the energy storage capability was demonstrated with a high energy density. Further adjustments to improve the performance of this system especially concerning the use of other membrane materials are currently ongoing.

Conflicts of interest

There are no conflicts to declare.

Acknowledgements

Funding of this project (tubulAir±, FKZ 03SF0436C) by the Bundesministerium für Bildung und Forschung is gratefully acknowledged. The authors thank Uta Sazama for TGA-MS and DSC measurements, Dr Daniel Szopinski for rheological experiments and Dr Bernhard Bugenhagen for solving the crystal structure.

Notes and references

1 Z. Yang, J. Zhang, M. C. W. Kintner-Meyer, X. Lu, D. Choi, J. P. Lemmon and J. Liu, *Chem. Rev.*, 2011, **111**, 3577.
2 L. Li, S. Kim, W. Wang, M. Vijayakumar, Z. Nie, B. Chen, J. Zhang, G. Xia, J. Hu, G. Graff, J. Liu and Z. Yang, *Adv. Energy Mater.*, 2011, **1**, 394.
3 K. M. Abraham, *J. Phys. Chem. Lett.*, 2015, **6**, 830.
4 J. W. Choi and D. Aurbach, *Nat. Rev. Mater.*, 2016, **1**, 16013.
5 B. Huskinson, M. P. Marshak, C. Suh, S. Er, M. R. Gerhardt, C. J. Galvin, X. Chen, A. Aspuru-Guzik, R. G. Gordon and M. J. Aziz, *Nature*, 2014, **505**, 195.
6 T. Janoschka, N. Martin, U. Martin, C. Friebe, S. Morgenstern, H. Hiller, M. D. Hager and U. S. Schubert, *Nature*, 2015, **527**, 78.
7 B. Hu, C. DeBruler, Z. Rhodes and T. L. Liu, *J. Am. Chem. Soc.*, 2017, **139**, 1207.
8 K. Gong, Q. Fang, S. Gu, S. F. Y. Li and Y. Yan, *Energy Environ. Sci.*, 2015, **8**, 3515.
9 X. Wei, W. Duan, J. Huang, L. Zhang, B. Li, D. Reed, W. Xu, V. Sprenkle and W. Wang, *ACS Energy Lett.*, 2016, **1**, 705.
10 J. Luo, B. Hu, C. DeBruler and T. L. Liu, *Angew. Chem., Int. Ed.*, 2018, **57**, 231.
11 A. M. Kosswattaarachchi and T. R. Cook, *Electrochim. Acta*, 2018, **261**, 296.
12 J. Winsberg, T. Hagemann, T. Janoschka, M. D. Hager and U. S. Schubert, *Angew. Chem., Int. Ed.*, 2017, **56**, 686.
13 L. E. VanGelder, A. M. Kosswattaarachchi, P. L. Forrestel, T. R. Cook and E. M. Matson, *Chem. Sci.*, 2018, **9**, 1692.
14 J. M. Stauber, S. Zhang, N. Gvozdik, Y. Jiang, L. Avena, K. J. Stevenson and C. C. Cummins, *J. Am. Chem. Soc.*, 2018, **140**, 538.
15 C. S. Sevov, K. H. Hendriks and M. S. Sanford, *J. Phys. Chem. C*, 2017, **121**, 24376.
16 C. DeBruler, B. Hu, J. Moss, J. Luo and T. L. Liu, *ACS Energy Lett.*, 2018, **3**, 663.
17 A. Mukhopadhyay, J. Hamel, R. Katahira and H. Zhu, *ACS Sustainable Chem. Eng.*, 2018, **6**, 5394.
18 W. Duan, X. Wei, *et al.*, *ACS Energy Lett.*, 2017, **2**, 1156.
19 M. Hayyan, F. S. Mjalli, M. A. Hashim, I. M. AlNashef and T. X. Mei, *J. Ind. Eng. Chem.*, 2013, **19**, 106.
20 A. A. J. Torriero, *Electrochemistry in Ionic Liquids*, Springer International Publishing, Cham, 2015.
21 S. Schaltin, Y. Li, N. R. Brooks, J. Sniekers, I. F. J. Vankelecom, K. Binnemans and J. Fransaer, *Chem. Commun.*, 2016, **52**, 414.
22 T. M. Anderson, D. Ingersoll, C. Staiger and H. Pratt, Sandia Corporation, *US* 9123943B1, 2015.
23 T. Nokami, T. Ito, H. Sakaguchi and H. Usui, Tottori Univ., *JP* 2016033117A, 2016.
24 H. D. Pratt III, N. S. Hudak, X. Fang and T. M. Anderson, *J. Power Sources*, 2013, **236**, 259.
25 Y. Liu, S. Lu, H. Wang, C. Yang, X. Su and Y. Xiang, *Adv. Energy Mater.*, 2017, **7**, 1601224.
26 J. Friedl, M. V. Holland-Cunz, F. Cording, F. L. Pfanschilling, C. Wills, W. McFarlane, B. Schricker, R. Fleck, H. Wolfschmidt and U. Stimming, *Energy Environ. Sci.*, 2018, **11**, 3010.
27 L. E. VanGelder and E. M. Matson, *J. Mater. Chem. A*, 2018, **6**, 13874.
28 J.-J. Chen, M. D. Symes and L. Cronin, *Nat. Chem.*, 2018, **10**, 1042.
29 L. E. VanGelder, B. E. Petel, O. Nachtigall, G. Martinez, W. W. Brennessel and E. M. Matson, *ChemSusChem*, 2018, **11**, 4139.

30 M. Milton, Q. Cheng, Y. Yang, C. Nuckolls, R. H. Sánchez and T. J. Sisto, *Nano Lett.*, 2017, **17**, 7859.
31 J. Friedl, M. A. Lebedeva, K. Porfyrakis, U. Stimming and T. W. Chamberlain, *J. Am. Chem. Soc.*, 2018, **140**, 401.
32 C. S. Sevov, S. L. Fisher, L. T. Thompson and M. S. Sanford, *J. Am. Chem. Soc.*, 2016, **138**, 15378.
33 H. Beinert, *Science*, 1997, **277**, 653.
34 P. Wasserscheid and T. Welton, *Ionic Liquids in Synthesis*, Wiley-VCH Verlag GmbH & Co. KGaA, Weinheim, 2007.
35 M. Watanabe, M. L. Thomas, S. Zhang, K. Ueno, T. Yasuda and K. Dokko, *Chem. Rev.*, 2017, **117**, 7190.
36 S. Sowmiah, V. Srinivasadesikan, M.-C. Tseng and Y.-H. Chu, *Molecules*, 2009, **14**, 3780.
37 C. Maton, N. de Vos and C. V. Stevens, *Chem. Soc. Rev.*, 2013, **42**, 5963.
38 O. Zech, A. Stoppa, R. Buchner and W. Kunz, *J. Chem. Eng. Data*, 2010, **55**, 1774.
39 A. Stoppa, O. Zech, W. Kunz and R. Buchner, *J. Chem. Eng. Data*, 2010, **55**, 1768.
40 B. Kirchner, *Ionic Liquids*, Springer, Berlin, Heidelberg, 2010.
41 M. V. Fedorov and A. A. Kornyshev, *Chem. Rev.*, 2014, **114**, 2978.
42 A. Ejigu, P. A. Greatorex-Davies and D. A. Walsh, *Electrochem. Commun.*, 2015, **54**, 55.
43 J. Noack, J. Tübke and K. Pinkwart, Fraunhofer Gesellschaft, *EP* 2399317B1, 2010.
44 P. G. Rickert, M. R. Antonio, M. A. Firestone, K.-A. Kubatko, T. Szreder, J. F. Wishart and M. L. Dietz, *J. Phys. Chem. B*, 2007, **111**, 4685.
45 A. B. Bourlinos, K. Raman, R. Herrera, Q. Zhang, L. A. Archer and E. P. Giannelis, *J. Am. Chem. Soc.*, 2004, **126**, 15358.
46 S. S. Mal, O. Tröppner, I. Ivanović-Burmazović and P. Burger, *Eur. J. Inorg. Chem.*, 2013, **2013**, 1960.
47 G. Christou and C. D. Garner, *J. Chem. Soc., Dalton Trans.*, 1979, 1093.
48 G. Yu, D. Zhao, L. Wen, S. Yang and X. Chen, *AIChE J.*, 2012, **58**, 2885.
49 CCDC 1573435† contains the supplementary crystallographic data for this paper.
50 V. R. Pallem and R. H. Holm, *Chem. Rev.*, 2004, **104**, 527.
51 M. Blesic, M. Swadźba-Kwaśny, T. Belhocine, H. Q. N. Gunaratne, J. N. C. Lopes, M. F. C. Gomes, A. A. H. Pádua, K. R. Seddon and L. P. N. Rebelo, *Phys. Chem. Chem. Phys.*, 2009, **11**, 8939.
52 K. J. Fraser, E. I. Izgorodina, M. Forsyth, J. L. Scott and D. R. MacFarlane, *Chem. Commun.*, 2007, **39**, 3817.
53 D. R. MacFarlane, M. Forsyth, E. I. Izgorodina, A. P. Abbott, G. Annat and K. Fraser, *Phys. Chem. Chem. Phys.*, 2009, **11**, 4962.
54 F. Rahman and M. Skyllas-Kazacos, *J. Power Sources*, 2009, **189**, 1212.
55 R. S. Nicholson, *Anal. Chem.*, 1965, **37**, 1351.
56 C. Choi, S. Kim, R. Kim, Y. Choi, S. Kim, H.-y. Jung, J. H. Yang and H.-T. Kim, *Renewable Sustainable Energy Rev.*, 2017, **69**, 263.
57 I. L. Escalante-Garcia, J. S. Wainright, L. T. Thompson and R. F. Savinell, *J. Electrochem. Soc.*, 2014, **162**, A363–A372.
58 R. H. Holm and W. Lo, *Chem. Rev.*, 2016, **116**, 13685.
59 K. S. Hagen, J. G. Reynolds and R. H. Holm, *J. Am. Chem. Soc.*, 1981, **103**, 4054.
60 G. Lin, P. Y. Chong, V. Yarlagadda, T. V. Nguyen, R. J. Wycisk, P. N. Pintauro, M. Bates, S. Mukerjee, M. C. Tucker and A. Z. Weber, *J. Electrochem. Soc.*, 2015, **163**, A5049–A5056.
61 M. C. Tucker, K. T. Cho, F. B. Spingler, A. Z. Weber and G. Lin, *J. Power Sources*, 2015, **284**, 212.
62 Q. Chen, L. Eisenach and M. J. Aziz, *J. Electrochem. Soc.*, 2015, **163**, A5057–A5063.
63 M. B. Freeman, Le Wang, D. S. Jones and C. M. Bejger, *J. Mater. Chem. A*, 2018, **6**, 21927.